Journal of Intelligent & Robotic Systems (2020) 98:627–641
https://doi.org/10.1007/s10846-019-01071-5

A Robust Linear Control Strategy to Enhance Damping of a Series Elastic Actuator on a Collaborative Robot

S. Ghidini[1] · M. Beschi[1] · N. Pedrocchi[1]

Received: 25 February 2019 / Accepted: 25 July 2019 / Published online: 16 August 2019

Abstract

Dealing with the physical interaction between humans and robots, Series Elastic Actuators (SEAs) are identified as one solution to overcome many limits, such as reducing contact forces or detect collisions. Nevertheless, the low-damping dynamic of a SEA can lead to undesired behaviours, especially during particular applications where a high level of precision is required. In this paper, a linear control architecture to enhance the damping performance of a SEA is presented. The proposed structure consists in a cascade control where loops are regulated using three types of controllers: PI, PD and a generalized controller specifically designed to damp oscillations. A frequency-domain approach with related constraints could not satisfy the time-domain goal in term of oscillation damping, for this reason an optimization problem able to consider them both is taken into account. A robust design is mandatory to the model mismatch introduced by neglecting coupling between motor. Therefore, robustness constraints are introduced in the optimization procedure. Indeed, the effectiveness of the control architecture is tested on a real compliant robot with six degrees of freedom equipped with as many SEAs. Each test aims to highlight the damping performance of the controlled system while the robot performs various tasks or it is subject to external disturbances.

Keywords Collaborative robots · Tuning rules · Series elastic actuator · Damped control · Robust control

1 Introduction

Human-robot interaction (HRI) has become a rapidly expanding field that involves a plethora of activities and researches [1]. Novel approaches to achieve a natural physical interaction continue to be presented [2, 3] however, the main aspects about safety and dependability should always be considered. From this point of view, a standard collaborative robot presents a reduced manipulator link inertia and a lightweight structure [4]. A large number of different proposals have been presented to overcome the limits imposed by the physical interaction between robots and humans (e.g reducing contact forces [5–7] and collisions detection/avoidance [8–10]). Compliant elements are also considered to increase robot safety. In particular, compliance is largely treated in bio-inspired robotics, as widely investigated in recent studies for legged [11, 12] and humanoid robots [13].

Compliant characteristics can be introduced by Series Elastic Actuators (SEAs) (e.g. SEAs-based humanoid robots [14]). Basically, a SEA is equipped with an elastic element in series with the couple motor-gearbox. In so doing, it is possible to reduce the overall rigidity and to contain the impact forces. Lately, as far as the authors know, the most prevalent applications of SEAs are related to the rehabilitation field ([17–19]), while industrial field applications are a recent field of interest, like peg-in-hole assembly [20] (where compliance facilitates the execution of the task), new grasping methods [21] or control structures for collaborative robots [22]. Benefits of SEAs in industrial environments are multiple, mainly related to inherent shock tolerance, high force fidelity and extremely low impedance, as treated in [15, 16]. Nevertheless, one of the main limit of SEAs are the evident oscillations created by the

✉ S. Ghidini
stefano.ghidini@stiima.cnr.it

M. Beschi
manuel.beschi@stiima.cnr.it

N. Pedrocchi
nicola.pedrocchi@stiima.cnr.it

[1] Institute of Intelligent Industrial Technologies and Systems for Advanced Manufacturing, National Research Council of Italy, Via A.Corti 12, 20133, Milan, Italy

elastic element, which can lead difficulties in adjusting the load position. Such drawback, in contrast with the high advantages related to SEAs lead the authors to consider the use of a SEA-based robot to enhance its limitations in terms of oscillations stability. In fact, the aim of this paper is to develop a control architecture able to overcome these problems by exploiting part of the robust tuning procedure faced in [22] and improving the damping level of a SEA-based robot without degrading performance. In so doing tasks where high precision is required can be accomplished with limited oscillations.

The choice of a correct dynamic model is crucial when dealing with robot equipped with this type of actuators. In fact, a SEA manipulator is typically affected by several model mismatches:

- The inertia perceived by each joint strongly depends on both the robot's configuration. Moreover, robot model is a Multi-Input-Multi-Output (MIMO) coupled system, where the movement of each joint affect the dynamics of the other ones.
- The manipulator is not an isolated system, in fact the presence of a (possible unknown) payload change the dynamics model. A more significant model mismatch is introduced when the robot is interacting with an external environment, such as peg-in-hole applications or human-robot physical interaction [35]. Finally, collaborative robot are often mounted on lightweight supports, like workdesk, introducing an addition viscous-elastic element [35].
- The spring may presents non-linear characteristics, such as mechanical backlash and/or nonlinear relationship between force and deformation.
- Friction terms depend on temperature [23], moreover breakout friction needs complex model to be compensated adequately [24], especially in changing direction movements.
- The rigid model assumptions may not be a good hypothesis for the light structure of collaborative robot links.

One the one hand, the designer can cope with these aspects by means of model-based MIMO control strategy, which requiring complex modelling of the robotic cell. On the other hand, a SISO robust control algorithm can be used to avoid complex modelling. The pros of the second choice are the reduction modelling effort and linearity of the system while the cons is the performance reduction when the system works around its nominal conditions. It is worth stressing that a torque feedforward signal can be added when a model is available, increasing the SISO control algorithm performance without altering the stability properties.

In this paper, robust control strategies based on frequency-domain analysis as faced in [22] and [25] are considered. Thanks to the SISO model approximation, it is possible to use frequency-domain constraints (i.e., maximum sensitivity and phase margin) in the optimization stage. In so doing, non-linearity phenomena and disturbances are considered as model uncertainties and mismatches. A high level of robustness is required to cope with the model mismatch.

However, [22] does not address the problem related to the low-damping behaviour of a SEA. This dynamic phenomenon is relevant in many common situations such as: unexpected or rapid contacts with human or objects (comparable to an impulsive disturbance), rapid applications of an external payload (comparable to a step disturbance) or demanding trajectories (e.g. pick and place trajectories).

A cascade with PID (or similar) controllers tuned to fulfil frequency-domain constraints (maximum sensitivity, phase margin) could not satisfy the time-domain goal in term of oscillation damping and disturbance rejection. For this reason, time-domain constraints should be directly taken into account.

The proposed structure is a cascade control loop, with a standard PI controller that regulates the inner loop. The outer loop is tuned in two different configurations, using as many controllers: a classic PD and a generalized controller able to freely set the closed-loop poles in multiple positions, guaranteeing more design flexibility if compared with a PD controller. An illustrative scheme is shown in Fig. 1.

The paper is divided as follows: in Section 2 the dynamic model of a SEA and the tuning procedure are presented. Section 3 reports the main guidelines and specifications on the optimization algorithm. In Section 4 are described the

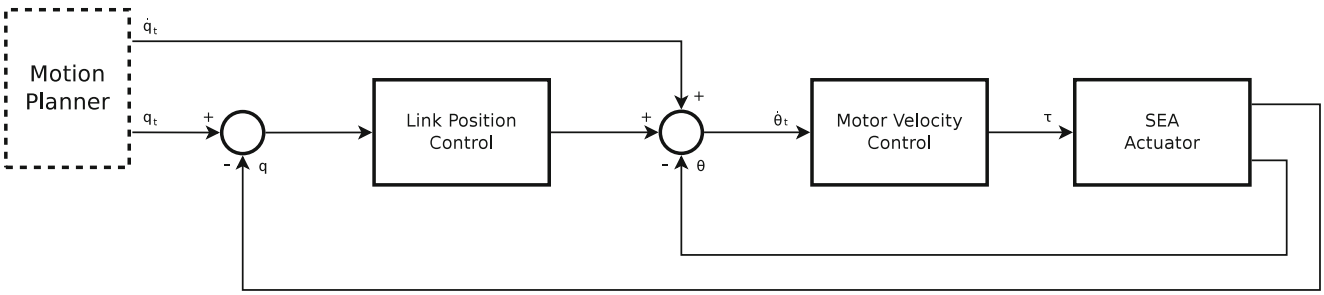

Fig. 1 Scheme of cascade control structure

experimental results of the control algorithm performed on a six degree of freedom compliant robot.

2 Methods

2.1 Dynamic Model of SEAs

A fair amount of SEA models consider the load positions as an external disturbance [26, 27], however a simplified linear SISO two mass model as the one described in [28] is enough to fit the main purposes of the paper, as described in Section 1.

In so doing, the dynamic model of a SEA includes three elements that define the joint: motor (with gearbox), spring and load. The robot is made by several SEAs connected in a open-chain kinematic. The coupling effects among actuators are considered as disturbances. Therefore, the controllers are tuned in decentralized fashion. Figure 2 shows a representative scheme of the joint structure with the main variables and parameters.

The position of the load q is defined as the sum of spring position δ and motor position θ (namely $q = \delta + \theta$). Obviously, a similar consideration is valid also for velocities and accelerations. J_m and J_l are the motor inertia and the load inertia. It is worth stressing that the proposed approach assumes known both the motor and load positions; in the experimental setup of Section 4, rotary encoders are used to measure these quantities. The terms k and h represent the elasticity and the viscosity of the elastic element between link and motor, while f_m and C_m represent, respectively, the viscous and Coulomb friction between motor and stator. Since C_m depends on the sign $\dot{\theta}$, the Coulomb friction is not directly taken into account in the model to preserve linearity. Therefore, it will be considered an external disturbance. Thus, it is possible to linearize the system by neglecting C_m and write a set of dynamic equations as follow:

$$\begin{cases} J_m\ddot{\theta} = h\dot{\delta} + k\delta - f_m\dot{\theta} + \tau \\ J_l(\ddot{\theta} + \ddot{\delta}) = -h\dot{\delta} - k\delta \end{cases} \tag{1}$$

That written in the Laplace domain becomes:

$$\begin{cases} J_m s_r^2\theta = hs_r\delta + k\delta - f_m s_r\theta + \tau \\ J_l s_r^2(\theta + \delta) = -hs_r\delta - k\delta \end{cases} \tag{2}$$

Where s_r is the complex variable for the real system. In fact, the quantity of parameters that appears in Eq. 2 can be reduced by mean of a model similitude for the sake of simplicity. In so on, a new set of variables with the same physical behaviour is introduced (In Eqs. 3 and 4 scaled model parameters are defined by an ˆsymbol):

$$s_r = \sqrt{\frac{k}{J_m}}\hat{s_r} \quad \theta = \frac{\hat{\theta}}{k} \quad \delta = \frac{\hat{\delta}}{k} \tag{3}$$

$$J_l = \hat{J}_l J_m \quad f_m = \hat{f}_m k\sqrt{\frac{J_m}{k}} \quad h = \hat{h}k\sqrt{\frac{J_m}{k}} \tag{4}$$

Thus, k and J_m are equal to 1, while the other scaled parameters can be found using the following conversion formulae (for more details, see Section 2.1 of [22]).

From her on out, the term $\hat{s_r}$ will be referred as s for the sake of simplicity. The same consideration is made for time t and frequency ω.

2.2 Tuning Procedure

While a plethora of applications involving SEAs and robots are commonly designed with impedance-control [29, 30] (e.g rehabilitation, robots assistive), the proposed control scheme resembles a cascade control where the secondary loop aims to regulate the velocity of the motor $\dot{\theta}$ and the primary loop regulates the position of the link q. As literature suggest [31] the inner loop is the first tuned, mainly considering disturbance rejection. Once the inner loop is tuned, it will be considered as the process for the primary. In so doing it is possible to tune the primary loop mainly considering trajectory tracking. Both the tuning procedures consist in minimizing a cost function by solving an optimization problem subjected to frequency- and time-domain constraints. Frequency-domain constraints are related to the maximum sensitivity M_s and the phase margin ϕ_m, they ensure enough level of robustness while

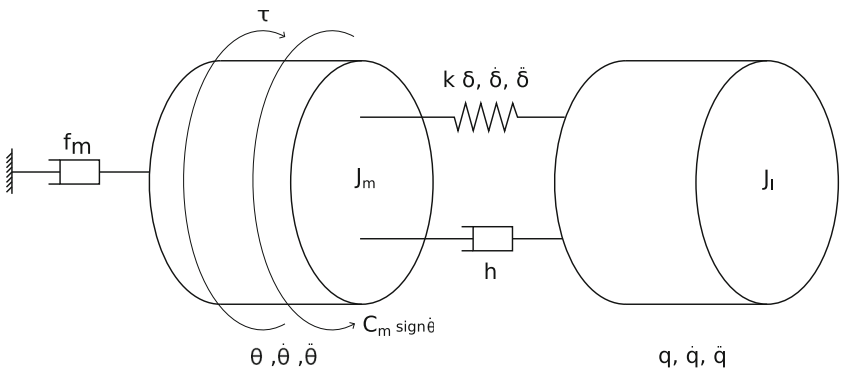

Fig. 2 Illustrative scheme of a series elastic actuator

the process is subject to parameters variations. The time-domain constraints ensure high levels of damping and disturbance rejection, as explained in more details in following sections.

2.3 Secondary Loop

The secondary loop is characterized by a faster dynamic and a large bandwidth, related to an aggressive controller. The aggressiveness is regulated by shaping the step-response $y(t)$ until a desired dynamic, described through a response $\hat{y}(t)$. At the same time, the robustness is ensured by imposing constraints on the frequency response. The desired response $\hat{y}(t)$ is defined by an exponential function. This choice is justified by two considerations. Firstly, an exponential function is generally easy to tune, and secondly it resembles the best theoretically behaviour when facing a step input signal, considering a system with maximum damping. Each response is described as follow:

$$y(t) = \mathcal{L}^{-1}\left[\frac{1}{s}\frac{P_{\dot{\theta},\tau}(s)C_v(s)}{1 + P_{\dot{\theta},\tau}(s)C_v(s)}\right] \tag{5}$$

$$\hat{y}(t) = 1 - e^{-\frac{t}{\tau}} \tag{6}$$

The cost function is defined as the difference between the response $y(t)$ to a unit step on the closed loop transfer function and a desired response $\hat{y}(t)$. The appropriate choice of $\hat{y}(t)$ determines faster or slower response and consequently the control dynamic. In Eq. 7 it is described the optimization problem structure.

$$cost = \int_0^\infty [y(t) - \hat{y}(t)]^2 dt$$
$$\text{such that: } \begin{cases} \min \phi_m \geq 45^\circ \\ \max M_s \leq 1.5 \\ \min |L(j\omega)| \geq 20dB \text{ if } \omega \leq 0.001\omega_r \left[\frac{rad}{s}\right] \\ \max |L(j\omega)| \leq -20dB \text{ if } \omega \geq 1000\omega_r \left[\frac{rad}{s}\right] \end{cases} \tag{7}$$

where ϕ_m is the phase margin, M_s is the maximum sensitivity, $L(j\omega) = P_{\dot{\theta},\tau}(j\omega)C_v(j\omega)$ is the loop transfer function and ω_r is the resonance frequency of the process. The constraints guarantee a satisfying level of robustness, while the cost function defines the aggressiveness level.

The controller is designed as a PI controller that rapidly reduces the motor velocity error and suppresses load disturbances. Its transfer function is defined as:

$$C_v(s) = K_p + \frac{K_i}{s} \tag{8}$$

where K_p is the proportional gain and K_i is the integral gain.

2.4 Primary Loop

While the inner loop presents an aggressive dynamic and aims to reject rapidly load disturbances, the primary loop reduces the load position error and limits oscillations. Amplitude and quantity of oscillations are regulated by shaping the closed loop response to a unitary impulse, until the desired dynamic is reached (less or more damped). An impulsive response is the simplest case in order to analyze oscillations produced and the decay ratio. In so doing, the optimization problem is designed similarly to the secondary loop, however the cost function is different. Basically, it aims to minimize the peaks of the closed loop impulse-response $y(t)$ by enveloping them with an exponential decreasing function $\hat{y}(t)$. Choosing correctly $\hat{y}(t)$, it is possible to control oscillations produced by the impulsive response, and thus, regulate the damping level of the system. It is worth stressing that in the proposed approach the desired damping in imposed by enveloping the closed-loop impulse response and not by adding a term, proportional to $(\dot{q} - \dot{\theta})$, to the motor torque.

Each response can be represented as follow:

$$y(t) = \mathcal{L}^{-1}\left[\frac{1}{s}\frac{P_{q,\tau}(s)C_p(s)}{1 + P_{q,\tau}(s)C_p(s)}\right] \tag{9}$$

$$\hat{y}(t) = e^{-\frac{t}{\tau}} \tag{10}$$

The peaks of the closed loop impulsive response enveloped through $\hat{y}(t)$ can be described through the set:

$$Q = \{z = |y(t)| \,\forall\, t \in [0, \infty) \,|\, y'(t) = 0 \wedge y''(t) \neq 0\} \tag{11}$$

Such a set is necessary to define the structure of the optimization problem as:

$$cost = \min \sum_{n=1}^{|Q|} z(t_n)\hat{y}(t_n)$$
$$\text{such that: } \begin{cases} \min \phi_m \geq 45^\circ \\ \max M_s \leq 3 \\ \min |L(j\omega)| \geq 20dB \text{ if } \omega \leq 0.001\omega_r \left[\frac{rad}{s}\right] \\ \max |L(j\omega)| \leq -20dB \text{ if } \omega \geq 1000\omega_r \left[\frac{rad}{s}\right] \\ \max Q \geq 0.1[rad] \end{cases} \tag{12}$$

Where t_n is the time calculated at the n_{th} peak and $|Q|$ is the cardinality of Q. Additionally, a new constraint ($\max Q \geq 0.1[rad]$) is introduced to set a limit on the smallest value that the maximum peak can assume. In this way it is possible to avoid very small peak amplitudes, related to an extremely slow and unsatisfactory response.

The controllers proposed are a standard PD and a generalized controller able to place closed-loop system poles in the desired positions, in order to overcome the limitations imposed by the PD. From here on out, it will be called "Poles Placement Controller" (PPC). The PD transfer function is defined as follow:

$$C_{p,PD}(s) = \frac{K_p + K_d s}{T_f s + 1} \tag{13}$$

While the design of the PPC needs some specific considerations.

2.5 Design of the PPC

In PPC controller, the closed-loop system poles are considered as control variable. In order to find the relation between the closed-loop system pole and the PPC transfer function parameter, the process of the inner loop is considered perfectly regulated (i.e. $\frac{\dot{\theta}(s)}{\tau(s)}$ with infinite bandwidth). If the motor velocity loop is correctly tuned, the hypothesis is acceptable and leads to simplify calculus. The open-loop process transfer function can be also defined using a notation with a damping ratio and natural frequency:

$$P_{q,\dot{\theta}}(s) = \frac{hs+k}{(J_l s^2 + hs + k)s} = \frac{1 + \xi \frac{s}{\omega_n}}{\left(1 + 2\xi \frac{s}{\omega_n} + \frac{s^2}{\omega_n^2}\right)s} \tag{14}$$

The controller poles are placed to fit the desired closed loop dynamic. Typically, a choice is to fix a desired closed loop transfer function $F(s)$ and find a controller able to model such $F(s)$. However, this situation may presents several problems. In fact, the controller transfer function depends on $F(s)$ and $P_{q,\dot{\theta}}(s)$:

$$C_{p,PPC}(s) = \frac{F(s)}{P_{q,\dot{\theta}}(s)[1 - F(s)]} \tag{15}$$

In ideal condition with the process $P_{q,\dot{\theta}}(s)$ perfectly modelled, the controller defined in Eq. 15 permits to obtain exactly the desired transfer function $F(s)$. In practice, it is never possible to obtain an ideal model as $P_{q,\dot{\theta}}(s)$. In this case, poles and zeros of the modelled process $P_{q,\dot{\theta}}(s)$ are introduced in the real closed loop transfer function (defined as $F_r(s)$) through the designed controller $C_{p,PPC}(s)$, as shown by:

$$F_r(s) = \frac{P_r(s)C_{p,PPC}(s)}{1 + P_r(s)C_{p,PPC}(s)} \tag{16}$$

Where $P_r(s)$ is the real process and $C_{p,PPC}(s)$ contains the modelled process $P_{q,\dot{\theta}}(s)$, as defined in Eq. 15. It is clear that $C_{p,PPC}(s)$ brings in the real closed loop transfer function the dynamic of the modelled process $P_{q,\dot{\theta}}(s)$, typically slow and undesirable.

Another problem is related to the rejection of load disturbances. Following the same considerations made previously, the real load disturbance sensitivity function (defined as $R_r(s)$) will be affected by the undesired dynamic of the process $P_{q,\dot{\theta}}(s)$ through the controller $C_{p,PPC}(s)$, as follow:

$$R_r(s) = \frac{P_r(s)}{1 + P_r(s)C_{p,PPC}(s)} \tag{17}$$

To overcome these problems, simplify poles of $P_{q,\dot{\theta}}(s)$ with zeros of $C_{p,PPC}(s)$ is a procedure that must be avoided by imposing conditions on the closed loop transfer function design.

For a better understanding, it can be helpful to define the modelled process $P_{q,\dot{\theta}}(s)$ and the desired closed loop transfer function $F(s)$ using numerator and denominator terms, obtaining the following equations:

$$F(s) = \frac{N_F(s)}{D_F(s)} \quad P_{q,\dot{\theta}} = \frac{N_P(s)}{D_P(s)} \quad 1 - F(s) = \frac{N_{1-F}(s)}{D_{1-F}(s)} \tag{18}$$

Through Eq. 18 and considering that $D_F(s) = D_{1-F}(s)$, it is possible to rewrite the controller in Eq. 15 as:

$$C_{p,PPC}(s) = \frac{N_F(s)D_P(s)}{N_P(s)N_{1-F}(s)} \tag{19}$$

Now, it is possible to define a set of conditions that make the controller independent from $P_{q,\dot{\theta}}(s)$:

– Condition 1: Avoid zeros simplification in $C_{p,PPC}(s)$

$$N_F(s) = N_P(s)B(s) = \left(1 + 2\xi \frac{s}{\omega_n}\right)B(s) \tag{20}$$

– Condition 2: Avoid poles simplification in $C_{p,PPC}(s)$

$$N_{1-F}(s) = D_p(s)A(s) = \left(\frac{s^2}{\omega_n^2} + 2\xi \frac{s}{\omega_n} + 1\right)sA(s) \tag{21}$$

$B(s)$ and $A(s)$ are free polynomials necessary to model the controller (and the closed loop transfer function) as desired.

Additionally, considering (18),(20) and (21), and the fact that $D_F(s) = N_F(s) + N_{1-F}(s)$, the desired closed loop transfer functions becomes:

$$F(s) = \frac{\left(1 + 2\xi \frac{s}{\omega_n}\right)B(s)}{\left(1 + 2\xi \frac{s}{\omega_n}\right)B(s) + (\frac{s^2}{\omega_n^2} + 2\xi \frac{s}{\omega_n} + 1)sA(s)} \tag{22}$$

While through the previous conditions, the controller transfer function defined in Eq. 19 becomes:

$$C_{p,PPC}(s) = \frac{B(s)}{A(s)} \tag{23}$$

Lastly, a third condition is imposed on $F(s)$ to impose a unitary gain.

– Condition 3: Unitary gain

$$F(0) = \frac{N_F(0)}{D_F(0)} = \frac{B(0)}{B(0) + A(0)} = 1 \tag{24}$$

That can be write as:

$$\begin{aligned} B(0) &= B(0) + A(0) \\ A(0) &= 0 \end{aligned} \tag{25}$$

The term $B(0)$ becomes a free variable that is arbitrarily imposed equal to 1.

The degrees of $B(s)$ and $A(s)$ determine the number of extra poles and zeros placed by the controller and affecting $F(s)$ (as deducible from Eq. 22). To identify each degree, the following considerations have been performed. Considering Eq. 22:

$$\deg[N_F(s)] = \deg[B(s)] + 1 \tag{26}$$

$$\begin{aligned}\deg[D_F(s)] &= \max\{\deg[B(s)]+1, \deg[A(s)]+2\} \\ &= \deg[A(s)]+2 \end{aligned} \tag{27}$$

$$\begin{aligned}&\deg[A(s)]+2-\{\deg[B(s)]+1\}=n \\ &\deg[A(s)]=\deg[B(s)]+n-1 \end{aligned} \tag{28}$$

Where n is the relative order of $F(s)$. The minimum value of n must be equal to the relative order of $P_{q,\dot{\theta}}$ (in this case, it is equal to 2), otherwise $A(s)$ must reduce the grade of $D_F(s)$ resulting in not proper controller (considering (23)).

The number of free variables available is equal to: $n_{fv} = deg[A(s)] + deg[B(s)]$. To arbitrary set poles of $F(s)$ it is necessary to impose:

$$deg[A(s)]+2 = deg[A(s)]+deg[B(s)] \tag{29}$$

And consequently, from Eqs. 29 and 28:

$$deg[A(s)] = 1+n, \quad deg[B(s)] = 2 \tag{30}$$

The optimization algorithm will so find the poles of the controller, taking into account the structure specified in Eq. 23 with grades defined in Eq. 30. In proposed approach, $deg[A(s)]$ is imposed equal to 3 in order to have an additional level of freedom during the shaping of $C_{p,PPC}(s)$ and to obtain an strictly proper controller reducing the high-frequency noise effects. In this way, it is possible to rewrite (23) as:

$$C_{p,PPC}(s) = \frac{B(s)}{A(s)} = \frac{B_2 s^2 + B_1 s + 1}{A_4 s^3 + A_3 s^2 + A_2 s + A_1} \tag{31}$$

To satisfy all the previous conditions, several algebraic calculi lead the coefficients of $C_{p,PPC}(s)$ to assume the following structure:

$$\begin{aligned}
B_2 &= \frac{p_2\omega_n^2 - p_4\omega_n^4 + p_6\omega_n^6 + 4\xi^2 + 2p_5\omega_n^5\xi - 4p_6\omega_n^6\xi^2 - 2p_1\omega_n\xi}{\omega_n^2} \\
B_1 &= -\frac{2\xi - p_1\omega_n + p_3\omega_n^3 - p_5\omega_n^5 - 8\xi^3 + 4p_1\omega_n\xi^2 - 2p_2\omega_n^2\xi + 2p_6\omega_n^6\xi}{\omega_n} \\
A_4 &= p_6\omega_n^2 \\
A_3 &= \omega_n^2(p_5 - 2p_6\omega_n\xi) \\
A_2 &= \omega_n^2(p_4 - p_6\omega_n^2 + 4p_6\omega_n^2\xi^2 - 2p_5\omega_n\xi) \\
A_1 &= \frac{p_3\omega_n^3 - p_5\omega_n^5 - 8\xi^3 + 4p_1\omega_n\xi^2 - 2p_2\omega_n^2\xi + 2p_6\omega_n^6\xi}{\omega_n}
\end{aligned} \tag{32}$$

Where p_1, p_2, p_3, p_4, p_5, p_6, namely the poles of $F(s)$, are the tuning parameters that will be found by solving the optimization problem.

3 Guidelines on the Optimization Algorithm

The optimization algorithm aims to find the best tuning parameters for the controllers that minimize the costs defined in Eqs. 7 and 12. In this way, the controllers designed previously depend on the parameters found by the solver. In other terms, considering the code implementation of the algorithm, it is possible to describe (5) and (9) as a function of the variable x_n:

$$C_v(s; x_1) \quad C_p(s; x_2) \tag{33}$$

where x_n is an array that contains the collection of the tuning parameters:

$$x_1 = \begin{bmatrix} K_p \\ K_i \end{bmatrix} \quad x_2 = \begin{bmatrix} p_1 \\ p_2 \\ p_3 \\ p_4 \\ p_5 \\ p_6 \end{bmatrix} \tag{34}$$

And the costs described in Eqs. 7 and 12 become the following functions:

$$\begin{aligned}
f(x_1) &= \int_0^\infty [y(t; x_1) - \hat{y}(t)]^2 \\
f(x_2) &= \min \sum_{n=1}^{|Q|} z(t_n; x_2)\hat{y}(t_n)
\end{aligned} \tag{35}$$

The algorithm was run on *Matlab* using a standard laptop equipped with an Intel i7-7700HQ CPU @ 2.80GHz ×8 and 16GB of RAM. All the controller parameters are found in completely offline manner. Since the optimization problem is designed to create robust controllers, a single set of parameters is enough to cover different scenarios. In this way a single offline approach before configuring the robot is necessary and sufficient to satisfy our purposes. Since the optimization problem is not convex, it was considered a multistart algorithm with 5 random initial conditions for the secondary loop and 10 random initial conditions for the primary. A function tolerance equal to 0.003 is considered. The constraints on the cost function ensure an adequate level of robustness. In so on, for each algorithm iteration the process parameters are fixed. The total execution time has a mean of 20[s] on the secondary loop, 45[s] on the primary loop using the PPC and 30[s] using the PD controller. It is

Table 1 Variation of parameter λ as a function of joints

	Joint							
	1		2		3	4	5	6
State	1	2	1	2	1	1	1	1
ω_{ar}	0.436	0.253	0.260	0.214	0.652	3.31	4.32	3.31
$1/\lambda_1$	3	3	3	3	3	3	3	3
$1/\lambda_2$	300	300	300	300	300	300	300	300

possible to evince how solving the problem using an online approach is not possible due to the heavy computational burden.

3.1 Specifications on the Time Constant τ

The time constant τ, namely how rapidly the exponential function $\hat{y}(t)$ evolves, is the main tuning parameter of the problem. It can be defined as:

$$\tau = \frac{\lambda}{\hat{\omega}_{ar}} \tag{36}$$

Where ω_{ar} is the antiresonace frequency and λ is a tuning parameter that influences the value of τ and the shape of the exponential function. The reason of choosing τ as defined in Eq. 36 is to model a simple parameter able to scale the exponential function for every joint. In fact, each joint is defined with the same model structure, however the parameters in Eq. 2 depend on the actuator, thus the exponential function must be correctly adapted for each joint. The dynamic model of a SEA is a dual inertia model with spring and damp, which presents a resonance/antiresonace effect on specific frequencies. The antiresonace frequency ω_{ar} is quantity that weight the most in the scaled problem, while the other parameters do not strong influence it.

About ω_{ar}, it is defined as:

$$\hat{\omega}_{ar} = \sqrt{\frac{\hat{k}}{\hat{J}_l}} \tag{37}$$

However, remembering that $\hat{k} = 1$ through the simplifications in Eq. 3, Eq. 4, it is possible to obtain:

$$\hat{\omega}_{ar} = \frac{1}{\sqrt{\hat{J}_l}} \tag{38}$$

The tuning parameter λ is specified as $\lambda = \lambda_2$ for the secondary loop and $\lambda = \lambda_1$ for the primary loop. Varying these values allows the user to regulate the aggressiveness of the controllers in a understandable way.

Considering the secondary loop, small values of λ_2 produce a response similar to $\hat{y}(t)$ with limited overshoot and slow dynamic. On the other hand, increasing λ_2 means faster dynamic with significant deviation from $\hat{y}(t)$ and greater overshoot.

On the primary loop, λ_1 defines how to model the envelop through the function $\hat{y}(t)$. Small values of λ_1 reduce the decay time of $\hat{y}(t)$, therefore, first peaks will present

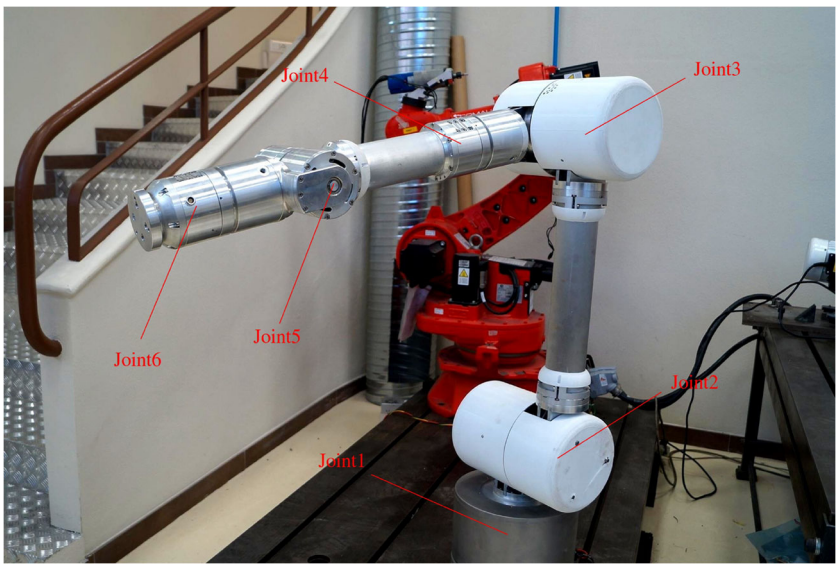

Fig. 3 Collaborative robot used in the context for testing the control structures. It is equipped with one SEA for each joint

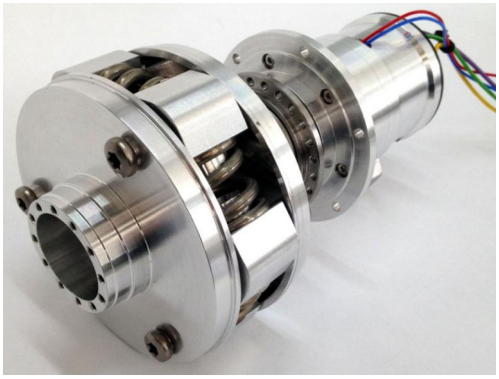

Fig. 4 Structure of a SEA used for the robot (Source: DFKI GmbH, with permission). It is designed with a fail safemechanical brake and a harmonic drive gear. The elasticity is generated by springs connected between the inner part of the actuator and the external structure

larger amplitudes. In so doing, the latter ones are more weighted by the optimization algorithm. On the other hand, high values of λ_1 increase the decay time of $\hat{y}(t)$. In this case also the last peaks will be enlarged, consequently, the optimization algorithm will weight mostly also the related amplitudes. In summary, different values of λ_1 lead to a trade-off between quantity and amplitude of peaks.

For the robot used in the experimental result, λ_1 and λ_2 are tuned as in Table 1 (Where λ is referred as $1/\lambda$ for a better readability). The chosen values of λ have a physical meaning that reflects the previous considerations about the trade-off between limited overshoot and aggressiveness. In this work, the same values of λ permit to obtain satisfy results. However, since the inertia may vary significantly depending on robot configuration, there are cases where the optimization algorithm will find parameters that are not physically compatible with the structure of actuators (e.g. bandwidth too high). In this situations, an ad-hoc choose of λ for a specific joint is the more practice solution. In general, it can be affirm that when the difference of ω_{ar} is significant among all the joints, an ad-hoc tuning is necessary. All the experimental results are taken with the values of Table 1.

3.2 Specifications on the Constraints

Observing the constraints in Eq. 7, the phase margin and the maximum sensitivity present standard values typical of a robust system: in fact, the secondary loop have to ensure robustness on the entire structure. On the other hand, observing (11), the primary loop does not need to add extra robustness. In so doing, the robust constraints are less stringent ($M_s \leq 3$), guaranteeing more freedom on the search of controller parameters. The minimum and maximum values on $|L(j\omega)|$ are imposed to constrain the shape of $L(s)$. In this way $L(s)$ is forced to have the minimum required structure that permits the reference tracking and disturbances rejection. Increasing the constraints values may limit the range of possibilities for the controller parameters. An approach is to fix a maximum and minimum frequency (e.g. around $1000\omega_r$ and $0.001\omega_r$) and impose small values of minimum and maximum $|L(j\omega)|$ at that frequencies (e.g. around $-20dB$ and $20dB$).

4 Experimental Results

Each control method has been tested on a six degree of freedom compliant robot (Fig. 3), developed for the European project FourByThree (FourByThree, 2018).

It is composed by six SEAs (a single one is shown in Fig. 4), composed by a brushless DC motors, a harmonic drive and an elastic element whose structure depends on the actuator considered.

Table 2 Parameters of the joint model

Parameters	Joint							
	1		2		3	4	5	6
$State$	1	2	1	2	1	1	1	1
$J_m\left[Kgm^2\right]$	4.59	7.21	6.77	8.48	2.65	0.0739	0.13	0.0869
$\hat{J_m}\left[Kgm^2\right]$	[−]	[−]	[−]	[−]	[−]	[−]	[−]	[−]
$J_l\left[Kgm^2\right]$	5.27	15.6	14.8	21.8	2.35	0.0915	0.0536	0.0915
$\hat{J}_l\left[Kgm^2\right]$	1.15	2.16	2.19	2.57	0.887	1.24	0.412	1.05
$k\left[\frac{Nm}{rad}\right]$	1260	1260	2000	194	839	235	207	289
$\hat{k}\left[\frac{Nm}{rad}\right]$	[−]	[−]	[−]	[−]	[−]	[−]	[−]	[−]
$h\left[\frac{Nm}{rad/s}\right]$	4.73	4.44	38.9	24.7	7.25	0.591	1.39	0.591
$\hat{h}\left[\frac{Nm}{rad/s}\right]$	0.0622	0.0466	0.334	0.193	0.154	0.142	0.268	0.118
$f_m\left[\frac{Nm}{rad/s}\right]$	89.6	101	107	117	34.3	1.61	2.95	2.23
$\hat{f}_m\left[\frac{Nm}{rad/s}\right]$	1.18	1.06	0.92	0.912	0.727	0.386	0.569	0.445

ROS operating system (ROS, 2018) is used to manage torque control signals that command actuators with an update frequency of 1[kHz]. Motor and spring position and velocity signals are provided by two different encoders every 1 [ms], integrated in the actuators and interfaced with a FPGA board. The first one can measure the position after the gear while the second one measures the position after the elastic element. The model of the actuator is the one described in Eq. 1, with the parameters for each joint as show in Table 2.

The first three tests aim to quantify the damping performance of the robot while the controllers proposed are applied on the system. With the last trial, it is also possible to oversee a tracking performance during a practical low demanding trajectory. In so doing, four different trials have been performed. It is worth stressing that the coupling effects between motors act like a model mismatch, which is coped with the robust constraints introduced in Eqs. 7 and 12. Thus, no decoupling mechanisms are introduced. The tests can be performed while all the actuators are actived.

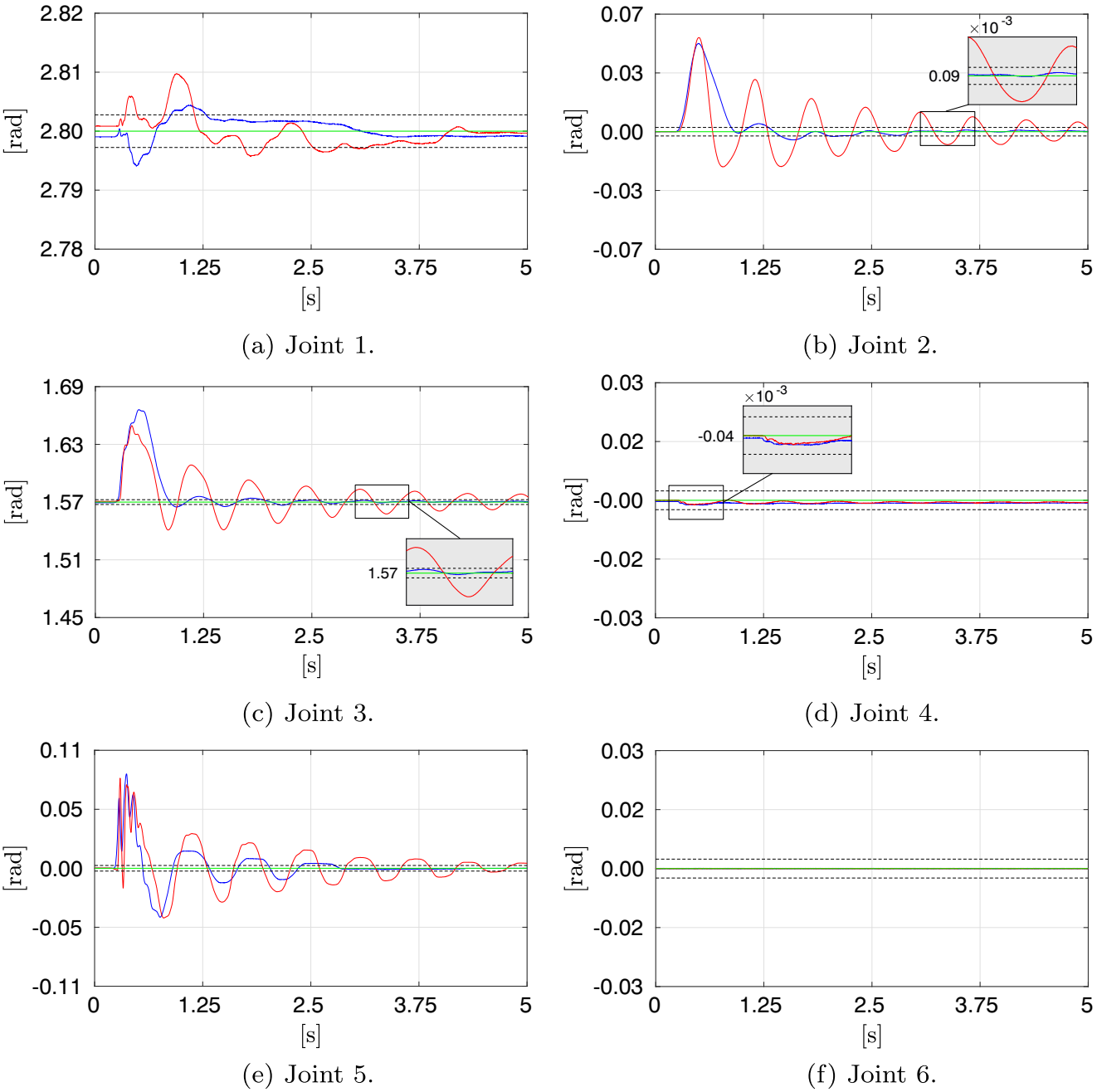

Fig. 5 Link position on trial 1: a 5[Kg] weight is applied on the end effector. Blue line: link position using the PPC. Red line: link position using the PD controller. Green line: set-point of the link position. Black dotted-line: 0.0025[rad]

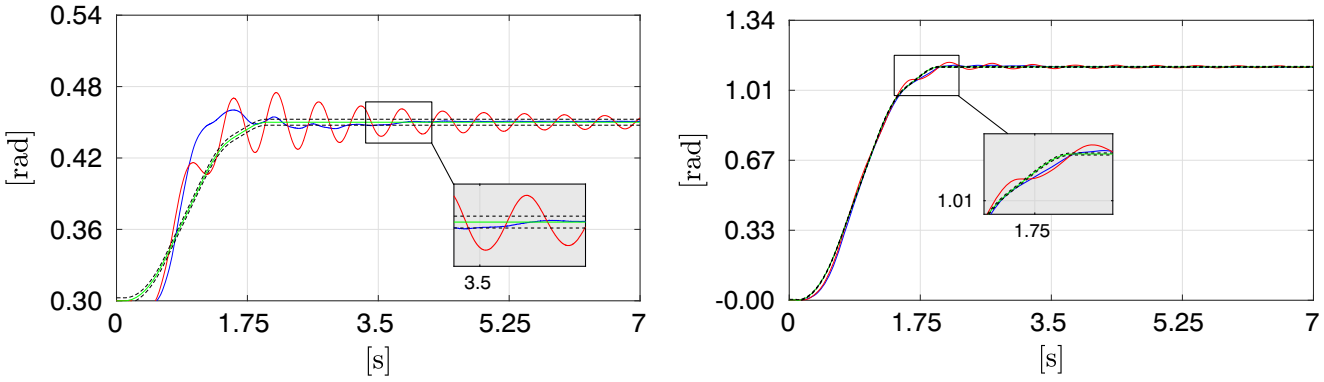

(a) Joint 2. (b) Joint 3.

Fig. 6 Link position on trial 2: Rapid vertical movement. Blue line: link position. Blue line: link position using PPC. Red line: link position using PD controller. Green line: set-point of the link position. Black dotted-line: 0.0025[rad]

Two trials are related to HRI contact scenarios, the first one simulates an impulsive force applied on the end-effector while the second one replies the appliance of a constant force. Other two trials are performed to evaluate tracking and damping level during a standard multi-joint trajectory and a more demanding one.

For each trial the PPC is compared with the classical PD controller in order to evidence strengths and weaknesses. The main significant results are obtain for joints 1-2-3-5, where the inertia perceived by the actuators is high enough to evaluate some difference between the PPC and PD controller. In fact, joints 4-6 are subject to very small variations and more complex controllers as the PPC are not strictly necessary. These considerations are observable also in the following experiments where joints 4-6 present small variations and comparable results both for the PPC and the PD. For every trail, a tolerance of 0.0025[rad] on the link position is considered. The choice of a 0.0025[rad] tolerance is related to the presence of a not modeled constant backlash for each joint, whose average is measured around 0.14°. Consequently a common effect during experiments is to observe the link position settle around such a value (e.g. after completion of the proposed tasks).

In the first trial a weight of 5[kg] is applied on the end-effector, trying to simulate a step disturbance. The load is applied at the same time both for the PPC and the PD controller. The most significant results are observed for joints 2 and 3, as shown in Fig. 5. Considering the second joint, the PPC is able to damp oscillations in almost 3[s], entering the tolerance range in . On the other hand, the link position waits more than 5[s] (almost 11[s]) to enter in the tolerance range with the PD controller. The third joint using the PPC takes 2.2[s] to enter the tolerance, while using the PD controller it must wait more than 5[s]. Joints 4-6 are affected just by small variations and noise.

The second trial consists in a rapid demanding trajectory along a vertical plane perpendicular to the floor with joints 1-4-5-6 fixed. In this case the robot lies almost along the vertical to the floor, and rapidly moves on the plane. Joint 2 is moved of 0.15 [rad] and joint 3 is moved of $\frac{\pi}{3}$ [rad]. This trajectory may simulate a rapid positioning of an object along a trajectory. This trial is highly significant to evaluate the performance of the PPC. In fact, observing Fig. 6, the PPC shows clearly better results. The link position enters the tolerance area almost in 3.5[s], while the PD controller needs definitely more than 5[s] (almost 12[s]).

The third trial simulates an impact with an object or the operator: in this case an impulsive force is rapidly applied on the end effector using a 1.5[kg] weight dropped from a height of 25[cm]. This test is similar to the first one, however the force applied resemble an impulsive disturbance. Also for this case, the PPC shows the best results. In Fig. 7 the PPC on joint 2 needs almost 1.3[s] to enter the tolerance zone, while the PD controller waits 5[s] to reach the tolerance, moreover oscillations continue persist. Joint 3 waits 2.9[s] with the PPC, while it takes near 5[s] with the PD controller. Joints 4-6 are affected just by small variations and noise.

The last trial consists in a low demanding trajectory performed on the entire workspace while all the joints are actuated. This test is not been performed to analyze the damping level provided by the controllers, instead, it aims to show up the overall tracking performance of the controller proposed, during a practical low demanding trajectory. The test can oversee such performance when there are significant coupling effects (namely, significant model

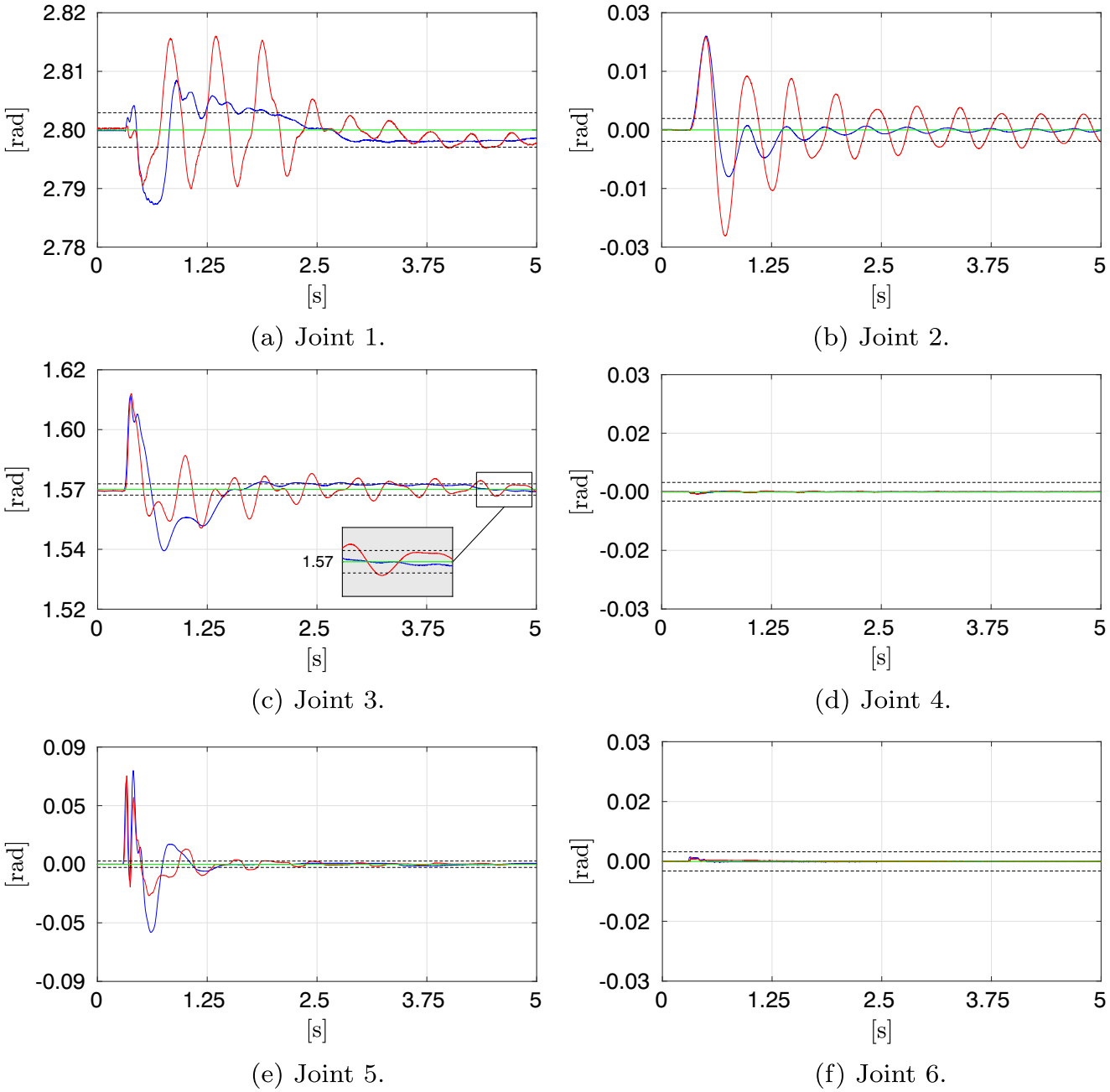

Fig. 7 Link position on trial 3: Rapid appliance of an impulsive force. Blue line: link position using the PPC. Red line: link position using the PD controller. Green line: set-point of the link position. Black dotted-line: 0.0025[rad]

mismatch from the controller point-of-view). Figure 8 shows trajectories comparison between the PPC and the PD controller, while Fig. 9 shows the related link position errors. By analyzing the plots it can be evinced that the trajectories are almost comparable (e.g. observing the enlarged area of joints 2-3). It is worth noticing that no torque feedforward signals are added to the controller output, resulting in a non zero tracking error during the trajectory evolution. When the robot dynamics model is available, the torque feedforward action can be added without affecting the controlled system stability and tuning procedure.

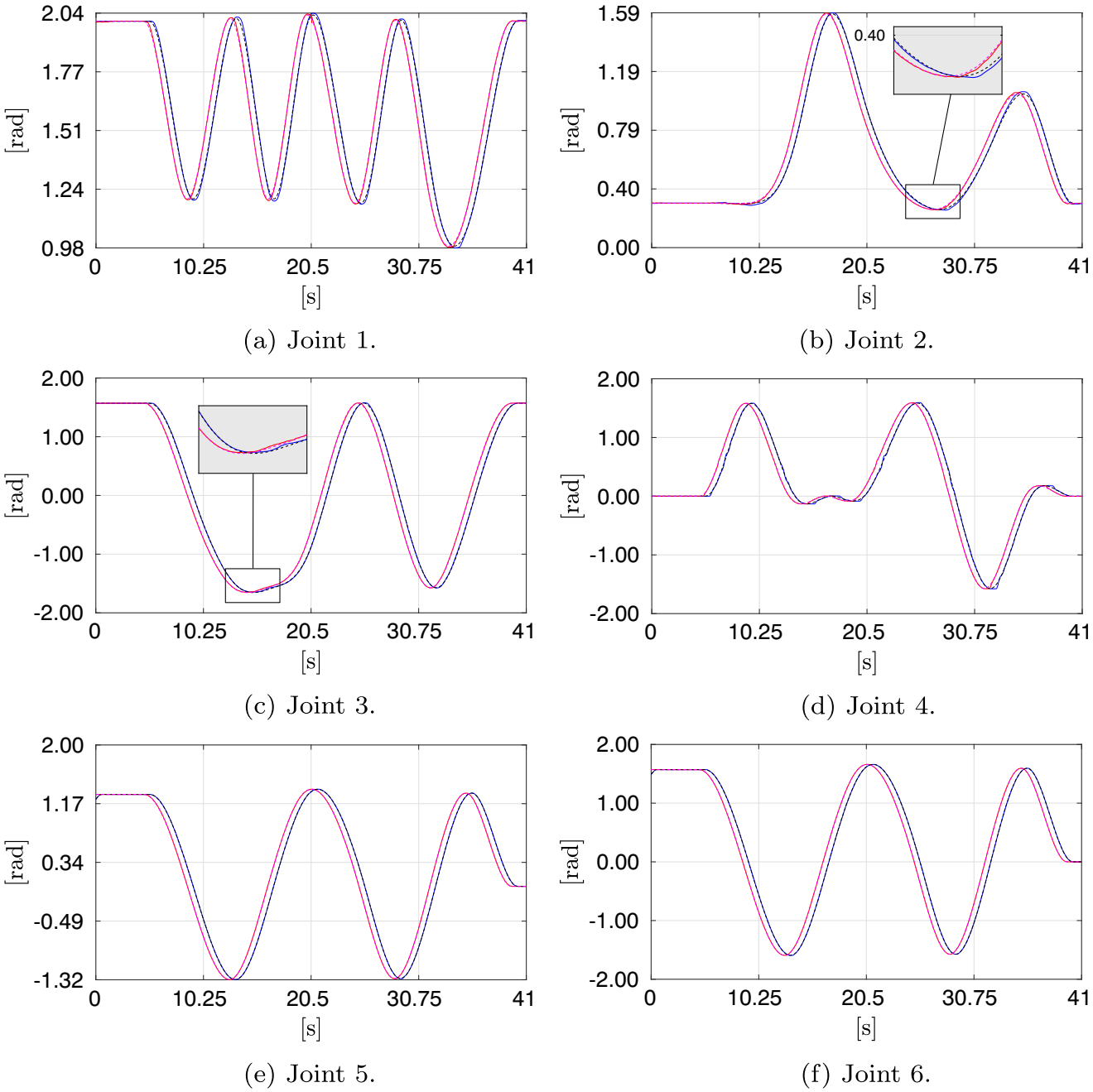

Fig. 8 Link position on trial 4: Trajectory on the entire workspace. Blue line: link position using the PPC. Black dotted-line: link position set-point using the PPC. Red line: link position using the PD controller. Magenta dotted-line: link position set-point using PD controller

In Table 3 are listed the main figures of merit (FOM) to evaluate the test: the mean absolute error $|\bar{e}|_p$ on the link position and the control effort c_e. Considering $|\bar{e}|_p$, the PD controller is the best choice for set-point tracking, although the PPC generally presents similar results. Moreover, the control effort c_e for the PPC presents lower values compared to the standard PD controller.

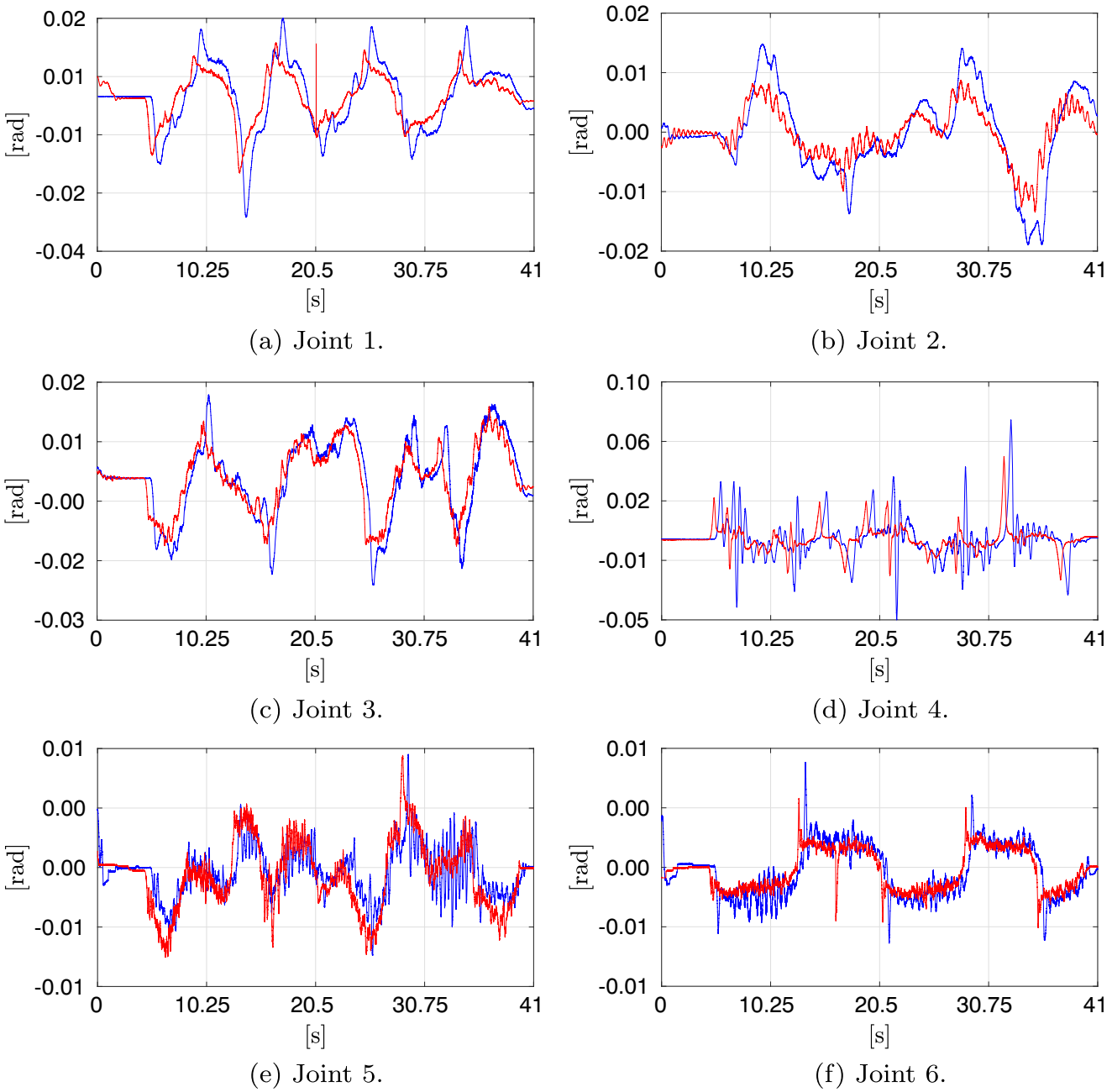

Fig. 9 Link position errors on trial 4. Blue line: link position error using the PPC. Red line: link position error using the PD controller

Table 3 Figures of merit (FOM) for trial 4

FOM	Controller	Joint					
		1	2	3	4	5	6
$\|\bar{e}\|_p$	PPC	0.00676	0.00539	0.00653	0.00792	0.00161	0.00190
	PD	0.00476	0.00321	0.00540	0.00477	0.00222	0.00152
c_e	PPC	1.97	0.866	2.44	0.205	0.237	0.352
	PD	3.35	1.47	4.27	0.358	0.397	0.712

5 Conclusions

The low-damping dynamic of a SEA can easily lead to inaccurate movements and undesired bumps. Tasks such as pick and place are hard to accomplish while maintaining a static pose free of oscillations. The contribution of this paper is to design a control structure able to improve the low-damping behaviour and enhance disturbances rejection by exploiting a time-domain analysis. The robust characteristics are ensured with a frequency-domain analysis as faced in [22]. A cascade structure is the control type used in the context. The secondary loop uses a PI controller, while the primary loop has been designed using a generalized controller (PPC) able to place closed-loop system poles in multiple positions, overcoming the limitations imposed by a standard PD and guaranteeing more degrees of freedom during controllers design.

An optimization problem is developed in order to find proper tuning parameters. Since strict robust constraints are imposed, a single set of parameters is enough to cover different scenarios. In so doing, an offline approach is necessary and sufficient. However, as a further researches, a background online re-tuning can be executed periodically at small frequencies to prevent excessive variations on the model due by aging effects. The heavy computational burden may limits an adaptive or online tuning while using the robust algorithm described, nevertheless a similar approach may cover aspects of HRI complementary with the offline optimization proposed. For example, SEA safety and assistance level can be enhanced by developing online event-trigger fuzzy methods, such as [32–34].

The only free tuning parameter considered is λ. A single value of λ is able to cover the ω_{ar} variations among all the joints. By varying λ it is possible to regulate desired levels of aggressiveness. Further researches may focus on automatic tuning methods to properly set λ depending on the desired response.

Four different tests have been performed to evaluate the efficiency of the control design. The first trial simulate a step disturbance by applying a 5[kg] load on the end effector. The second trial is a fast trajectory that simulates a rapid placing of an object along. The third trial may simulate the impact with a 1.5[kg] object, while the last trial consists in a trajectory performed along the whole workspace. The experimental results show how the PPC is able to damp oscillations even three/four times faster than a standard PD controller (demonstration video available in: [36]). However, considering only the mean absolute error, the classic PD controller presents better tracking performances during stressful trajectories. Merging both methods may be a starting point for further researches. In so doing a gain scheduling between the PD controller and the PPC could be a feasible solution.

Acknowledgments The work is partially supported by FourByThree Project H2020-FoF-06-2014-737095.

Compliance with Ethical Standards

Conflict of interests None declared.

References

1. Sheridan, T.B.: Human–robot interaction: status and challenges. Hum. Factors **58**(4), 525–532 (2016)
2. Nemec, B., Likar, N., Gams, A., Ude, A.: Human robot cooperation with compliance adaptation along the motion trajectory. Auton. Robot. **42**(5), 1023–1035 (2018)
3. Alqaudi, B., Modares, H., Ranatunga, I., Tousif, S.M., Lewis, F.L., Popa, D.O.: Model reference adaptive impedance control for physical human–robot interaction. Control Theory and Technology **14**(1), 68–82 (2016)
4. De Santis, A., Siciliano, B., De Luca, A., Bicchi, A.: An atlas of physical human–robot interaction. Mech. Mach. Theory **43**(3), 253–270 (2008)
5. Tian, Y., Chen, Z., Jia, T., Wang, A., Li, L.: Sensorless collision detection and contact force estimation for collaborative robots based on torque observer. In: 2016 IEEE international conference on robotics and biomimetics (ROBIO), pp. 946–951. IEEE (2016)
6. Fritzsche, M., Elkmann, N., Schulenburg, E.: Tactile sensing: A key technology for safe physical human robot interaction. In: Proceedings of the 6th international conference on human–robot interaction (pp. 139–140). ACM (2011)
7. Magrini, E., Flacco, F., De Luca, A.: Control of generalized contact motion and force in physical human–robot interaction. In: 2015 IEEE international conference on robotics and automation (ICRA), pp. 2298–2304. IEEE (2015)
8. Dimeas, F., Avendano–Valencia, L.D., Aspragathos, N.: Human–robot collision detection and identification based on fuzzy and time series modelling. Robotica **33**(9), 1886–1898 (2015)
9. Lee, S.D., Song, J.B.: Sensorless collision detection based on friction model for a robot manipulator. Int. J. Precis. Eng. Manuf. **17**(1), 11–17 (2016)
10. Lo, S.Y., Cheng, C.A., Huang, H.P.: Virtual impedance control for safe human–robot interaction. J. Intell. Robot. Syst. **82**(1), 3–19 (2016)
11. Machairas, K., Papadopoulos, E.: An active compliance controller for quadruped trotting. In: 2016 24th mediterranean conference on control and automation (MED) (pp. 743–748). IEEE (2016)
12. Pouya, S., Khodabakhsh, M., Sprowitz, A., Ijspeert, A.: Spinal joint compliance and actuation in a simulated bounding quadruped robot. Auton. Robot. **41**(2), 437–452 (2017)
13. Knabe, C., Seminatore, J., Webb, J., Hopkins, M., Furukawa, T., Leonessa, A., Lattimer, B.: Design of a series elastic humanoid for the DARPA Robotics Challenge. In: 2015 IEEE–RAS 15th international conference on humanoid robots (Humanoids) (pp. 738–743). IEEE (2015)
14. Tatsch, C., Ahmadi, A., Bottega, F., Tani, J., da Silva Guerra, R.: Dimitri: an Open–Source Humanoid Robot with Compliant Joint. J. Intell. Robot. Syst. **91**(2), 291–300 (2018)
15. Pratt, G.A., Williamson, M.M.: Series elastic actuators. In Intelligent Robots and Systems 95.'Human Robot Interaction and Cooperative Robots', Proceedings. 1995 IEEE/RSJ International Conference on (Vol. 1, pp. 399–406). IEEE (1995)
16. Paluska, D., Herr, H.: Series elasticity and actuator power output. In: Proceedings 2006 IEEE international conference on robotics and automation, 2006. ICRA 2006. (pp. 1830–1833). IEEE (2006)

17. Paine, N., Mehling, J.S., Holley, J., Radford, N.A., Johnson, G., Fok, C.L., Sentis, L.: Actuator control for the NASA JSC Valkyrie humanoid robot: A decoupled dynamics approach for torque control of series elastic robots. J. Field Rob. **32**(3), 378–396 (2015)
18. Zhang, Q., Xu, B., Guo, Z., Xiao, X.: Design and modeling of a compact rotary series elastic actuator for an elbow rehabilitation robot. In: International conference on intelligent robotics and applications (pp. 44–56). Springer, Cham (2017)
19. Yu, H., Huang, S., Chen, G., Pan, Y., Guo, Z.: Human robot interaction control of rehabilitation robots with series elastic actuators. IEEE Trans. Robot. **31**(5), 1089–1100 (2015)
20. Park, H., Park, J., Lee, D.H., Park, J.H., Baeg, M.H., Bae, J.H.: Compliance–based robotic peg–in–hole assembly strategy without force feedback. IEEE Trans. Ind. Electron. **64**(8), 6299–6309 (2017)
21. Deimel, R., Brock, O.: A novel type of compliant and underactuated robotic hand for dexterous grasping. Int. J. Robot. Res. **35**(1–3), 161–185 (2016)
22. Ghidini, S., Beschi, M., Pedrocchi, N., Visioli, A.: Robust Tuning Rules for Series Elastic Actuator PID Cascade Controllers. IFAC–PapersOnLine **51**(4), 220–225 (2018). https://doi.org/10.1016/j.ifacol.2018.06.069
23. Simoni, L., Beschi, M., Legnani, G., Visioli, A.: Modelling the temperature in joint friction of industrial manipulators. Robotica, 1–22 (2018)
24. Johanastrom, K., Canudas-de-Wit, C.: Revisiting the LuGre friction model. IEEE Control. Syst. Mag. **28**(6), 101–114 (2008). 10.1109/MCS.2008.929425
25. Wang, M., Sun, L., Yin, W., Dong, S., Liu, J.: Continuous robust control for series elastic actuator with unknown payload parameters and external disturbances. IEEE/CAA Journal of Automatica Sinica **4**(4), 620–627 (2017)
26. Grun, M., Muller, R., Konigorski, U.: Model based control of series elastic actuators. In: 2012 4th Ieee Ras & Embs international conference on biomedical robotics and biomechatronics (Biorob) (pp. 538–543). IEEE (2012)
27. Vallery, H., Veneman, J., Van Asseldonk, E., Ekkelenkamp, R., Buss, M., Van Der Kooij, H.: Compliant actuation of rehabilitation robots. IEEE Robot. Autom. Mag. **15**(3), 60–69 (2008)
28. Oh, S., Kong, K.: High–precision robust force control of a series elastic actuator. IEEE/ASME Trans. Mechatron. **22**(1), 71–80 (2017)
29. Calanca, A., Fiorini, P.: Impedance control of series elastic actuators based on well–defined force dynamics. Robot. Auton. Syst. **96**, 81–92 (2017)
30. Calanca, A., Muradore, R., Fiorini, P.: Impedance control of series elastic actuators: Passivity and acceleration–based control. Mechatronics **47**, 37–48 (2017)
31. Veronesi, M., Visioli, A.: Simultaneous closed–loop automatic tuning method for cascade controllers. IET Control Theory Appl. **5**(2), 263–270 (2011)
32. Qiu, J., Sun, K., Wang, T., Gao, H.: Observer-based fuzzy adaptive event-triggered control for pure-feedback nonlinear systems with prescribed performance. IEEE Transactions on Fuzzy Systems. https://doi.org/10.1109/TFUZZ.2019.2895560 (2019)
33. Roveda, L., Haghshenas, S., Prini, A., Dinon, T., Pedrocchi, N., Braghin, F., Tosatti, L.M.: Fuzzy impedance control for enhancing capabilities of humans in onerous tasks execution. In: 2018 15th international conference on ubiquitous robots (UR) (pp. 406-411). IEEE. https://doi.org/10.1109/URAI.2018.8441800 (2018)
34. Sun, K., Mou, S., Qiu, J., Wang, T., Gao, H.: Adaptive fuzzy control for non-triangular structural stochastic switched nonlinear systems with full state constraints. IEEE Transactions on Fuzzy Systems. https://doi.org/10.1109/TFUZZ.2018.2883374 (2018)
35. Roveda, L., Vicentini, F., Pedrocchi, N., Braghin, F., Tosatti, L.M.: Impedance shaping controller for robotic applications involving interacting compliant environments and compliant robot bases, Proceedings of IEEE International Conference on Robotics and Automation (ICRA), Seattle, WA, pp. 2066–2071. https://doi.org/10.1109/ICRA.2015.7139470 (2015)
36. Ghidini, S.: Damped Control for a SEA Collaborative Robot. Retrieved from https://www.youtube.com/watch?v=NGLLilA8rTE (2019)

S. Ghidini received his B.S. and M.S degrees in Industrial Automation Engineering from the University of Brescia in 2015 and 2017, respectively. In 2017 he also received the Master de Sciences et Technologie, mention Science de l'Ingenieur, specialized in advanced systems and robotics from the University Pierre and Marie Curie (Paris). Since November 2017 he is a research fellow with the National Research Council at the Institute of Intelligent Industrial Technologies and Systems for Advanced Manufacturing. His research interests include industrial robotics, industrial and automatic control, compliant robots, physical human-robot interaction and cooperation.

M. Beschi received his B.S. and M.S degrees in Industrial Automation Engineering from the University of Brescia in 2008 and 2010, respectively. In 2014, he received his Ph.D. degree in Computer Science, Engineering and Control Systems technologies at the University of Brescia, discussing a thesis about "Event-based and model-based control strategies with applications to solar energy systems". From June 2014 he is a researcher with the National Research Council at the Institute of Intelligent Industrial Technologies and Systems for Advanced Manufacturing. He is author of several scientific publications in international journals and conferences.

N. Pedrocchi received his Ph.D. degree in Applied Mechanics and Robotics at the University of Brescia in 2008, discussing a thesis about the force control for industrial robots in deburring applications.

From July 2011 he is a permanent researcher with the National Research Council of Italy at the Institute of Intelligent Industrial Technologies and Systems for Advanced Manufacturing. He is published several scientific publications in international journals and conferences on control and motion planning of industrial robots, as well as the adoption of robots in rehabilitation robotics and human assistance.